Heliyon 10 (2024) e37579

Contents lists available at ScienceDirect

Heliyon

journal homepage: www.cell.com/heliyon

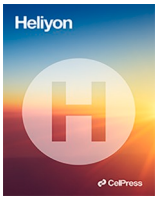

Research article

Physical-chemical characterisation of an alum-based water treatment sludge in different raw water turbidity scenarios

Camilo C. Castro-Jiménez *, Julio C. Saldarriaga-Molina, Edwin F. García

Escuela Ambiental, Facultad de Ingeniería, Universidad de Antioquia UdeA, Calle 70 No. 52-21, Medellín, Colombia

A R T I C L E I N F O

Keywords:
Circular economy
Drinking water treatment sludge
Physicochemical characterisation
Sludge management
Sludge production

A B S T R A C T

Characterisation of the water treatment sludge (WTS) generated in drinking water treatment plants (DWTPs) is crucial to define alternatives for its adequate management, including potential reuse options. To define these alternatives, it is necessary to evaluate rainfall seasonality effect on WTS production and its physical and chemical characteristics. This study assessed the production and characterisation of four types of alum-based WTS. The WTS was generated in a pilot-scale system from different raw water turbidities (i.e., low: <5 NTU, medium: 5–10 NTU, high: ≥10 NTU, and very high turbidity: ~300 NTU) and coagulant doses. To estimate WTS production, mathematical models based on variables such as raw water turbidity, coagulant dosage, and organic matter removed were used. The WTS characterisations included physical (solids and particle size distribution), chemical (metallic oxides, pH, mineral phases), and surface properties (functional groups and zero-charge point pH). The modified Kawamura model presented the best fit ($R^2 = 1.0$, RMSE = 0.1062 and the lower Akaike Information Criterion) for the estimation of WTS production, indicating that at the DWTPs, it is possible to make sludge production projections using only two simple variables: coagulant dose and the raw water turbidity. The four types of WTS consist mainly of amorphous materials (45–65 %), featuring some mineral phases and exhibiting high contents of Al (Al_2O_3: 30–34 %), Si (SiO_2: 21–26 %) and Fe (Fe_2O_3: 11–13 %). Nevertheless, very high turbidity WTS shows variations in its characteristics, notably a heightened content of clays. As a result of the high concentrations of Al and Fe, the WTS has the potential to be used as coagulants or for the recovery of coagulants, especially low turbidity WTS, which is produced from water with low turbidity and organic matter. The presence of aluminium–silicate clays and the surface functional groups of the silica network suggest that WTS, particularly very high turbidity WTS, also has the potential to be raw materials for generating adsorbents. The potential applications of WTS in coagulation and adsorption can be leveraged in wastewater treatment, promoting the circular economy in the water sector.

1. Introduction

The Sustainable Development Goals 11 and 12, defined by the United Nations, include among their targets the reduction of the adverse environmental impact of cities, with particular attention to waste management, focusing on strategies for its reduction, recycling and reuse [1]. The waste generated in cities and towns includes water treatment sludge (WTS), which is a by-product of

* Corresponding author.
E-mail address: camilo.castro@udea.edu.co (C.C. Castro-Jiménez).

https://doi.org/10.1016/j.heliyon.2024.e37579
Received 14 June 2024; Received in revised form 4 September 2024; Accepted 5 September 2024
Available online 6 September 2024

drinking water treatment [2]. In the 1990s, the global production of WTS was estimated to be 10,000 tonnes per day [3]. Due to population growth and economic development, global water consumption has increased [4], leading to a corresponding increase in the generation of WTS. Currently, the global daily generation of WTS is estimated to be 100,000 tonnes, and this production is projected to triple in the coming decades [5].

Conventional drinking water treatment plants (DWTPs) include coagulation/flocculation, sedimentation, filtration and disinfection processes [6]. DWTPs aim to eliminate colloidal and suspended impurities, natural organic matter (NOM), microorganisms, and other pollutants from water [7]. Aluminium (Al) and iron (Fe)-based chemicals are the most commonly employed coagulants in the coagulation/flocculation stage [8]. Among them, hydrolysable metal salts based on Al or Fe, such as aluminium sulphate or alum ($Al_2(SO_4)_3{\cdot}14H_2O$), are the most used coagulant due to their high efficiency and low cost [5]. Aluminium sulphate facilitates particle collision by neutralising charges and sweeping, leading to their destabilisation and subsequent agglomeration into larger aggregates. These aggregates are then separated through sedimentation and filtration [9]. The waste that accumulates at the bottom of sedimentation tanks is referred to as WTS. Inorganic contaminants (such as metals and metalloids), as well as organic contaminants (including NOM, bacteria, and algae), are constituents of WTS [2,10]. The volume of WTS produced by a DWTP is estimated to range between 1 % and 3 % of the total volume of raw water treated [11].

In developing countries, WTS is usually discharged directly into nearby water bodies, and dewatered WTS is disposed of in landfills [12]. Nevertheless, releasing WTS into water bodies affects water quality and ecology [13]. Currently, landfilling of WTS is no longer considered practical due to reduced available landfill sites and increased operating costs [14]. Additionally, recycling or reusing valuable elements or materials present in WTS is not feasible after their disposal in landfills [15]. Therefore, there is a need to develop strategies for the sustainable management of WTS within the context of the circular economy and the objective of zero waste, adhering to the 5R principles of waste management: reduce, reprocess, reuse, recycle and recover [11,16]. In this context, numerous studies on the reuse and recovery of WTS materials have been documented in the literature. Sharma and Ahammed [7] and Dias et al. [17] review various WTS applications as adsorbents for removing pollutants from water and wastewater. The study by Nayeri and Mousavi [18] reviews several alternatives for the recovery and reuse of coagulants from WTS, such as acidification, basification, ion-exchanging and electrodialysis [19–23]. De Carvalho Gomes et al. [24] present a review of the applications of WTS in construction materials. The work by Tony [16] also reviews alternative valorisation methods for WTS, including agricultural uses and their application as a substrate in constructed wetlands. Azeddine et al. [25] highlight the importance of the physicochemical characterisation of WTS in defining their applications in manufacturing different products (e.g., bricks or blocks) and in energy cogeneration.

Nevertheless, the production of WTS and its physicochemical composition depends on the quality of the raw water and the operational conditions in the associated DWTP, and it varies over time. Therefore, conducting qualitative and quantitative studies of the WTS produced in a DWTP is necessary and essential to define alternatives for its management, including potential reuse options [12,26]. To the authors' knowledge, few investigations have evaluated the characteristics of WTS generated under different raw water conditions and operational parameters during drinking water treatment. Nair and Ahammed [27] investigated the impact of raw water quality, coagulant type and dosage on WTS production at the laboratory scale, focusing on evaluating the efficiency of aluminium recovery from WTS through acidification. Their results indicate that higher concentrations of organic matter and turbidity in the raw water led to lower aluminium recovery efficiency. The authors highlight the significant effects of raw water quality, coagulant type and dose on the coagulant recovery process. In their study, Ahmad et al. [28] assessed the monthly WTS production using empirical equations at a DWTP in India over 12 months, encompassing various seasons, such as winter, pre-monsoon, monsoon and post-monsoon. The WTS generated during these four seasons were characterised by moisture, organic matter, pH, fixed solids and particle size distribution. The authors outlined that seasonal variations significantly impact the quality of raw water received at the DWTP, leading to variations in sludge generation. Finally, the authors emphasised the importance of quantifying and characterising the WTS produced at the DWTP to formulate appropriate management strategies for its economical and environmentally friendly disposal. Similarly, Nguyen et al. [29] emphasize the importance of identifying the viability in chemical and physical properties in a DWTP over a year.

This study aimed to assess the characterisation of four types of alum-based WTS generated under different raw water turbidity and coagulant doses in a DWTP. The WTS was produced in a pilot-scale coagulation, flocculation and sedimentation system, replicating the operational conditions of the DWTP for each raw water type. The tests involved basic characterisations of raw water, treated water and WTS. Sludge production was determined experimentally and through empirical models. Furthermore, analyses of chemical compounds (X-ray fluorescence - ED-XRF), mineral phases (X-Ray Diffraction Analysis - XRD), active surface functional groups (Fourier transform infrared spectroscopy - FTIR), zero-charge point pH (pH_{PZC}) (Solids addition method) and particle size distribution (Laser diffraction) were conducted on the four types of WTS, providing potential insights for their reuse and valorisation.

2. Methodology

2.1. Operative conditions of DWTPs

The WTS characterisation was conducted at a municipal DWTP in Colombia. This conventional DWTP treats surface water through coagulation, flocculation, sedimentation, rapid sand filtration and disinfection. Aluminium sulphate type A (alum) is used as the coagulant. According to its technical data sheet, type A alum contains a minimum of 17 % alumina (Al_2O_3) and a maximum of 0.008 % iron (Fe_2O_3) content. DWTP operators frequently conduct jar tests to determine the optimal coagulant dose, analysing variables such as the turbidity of the raw water and the remaining turbidity after the sedimentation stage of the jar test. Hence, a statistical analysis was conducted on the records of raw water turbidity, coagulant doses, and rainfall over five years of DWTP operation (i.e., 2016–2020).

Based on this analysis, three categories of WTS were established (i.e., low turbidity, medium turbidity and high turbidity), each linked to specific raw water turbidity (i.e., low: <5 NTU, medium: 5–10 NTU and high: ≥10 NTU) and the corresponding operational parameters of the DWTP (i.e., coagulant dose). Subsequently, a new category of raw water (very high turbidity: ~300 NTU) was introduced during the water sampling for conducting coagulant dose tests, leading to the inclusion of a fourth type of WTS in this study (i.e., very high turbidity). These four categories of raw water turbidity found through statistical analysis are specific to the DWTP studied and were not defined from existing literature.

2.2. Jar test for coagulation dosing

To validate the coagulant doses used in the DWTP for each WTS category, jar tests were conducted with raw water that had turbidity levels within the respective range associated with each category of WTS. Water sampling for jar tests was performed using a bucket in the DWTP inlet channel. The samples were immediately carried to the plant laboratory and deposited in the beakers of the jar equipment. The time elapsed between water sampling and the start of the tests was, at most, 30 min. The tests were conducted using a standard jar test apparatus (brand Phipps and Birds) with a sample volume of 2000 mL. Rapid mixing was carried out at 200 rpm for 1 min, followed by slow mixing for 20 min (13 min at 43 rpm, 2.5 min at 40 rpm and finally 4.5 min at 30 rpm). Subsequently, the jars were left undisturbed for 15 min to allow the flocs to settle [30]. Afterwards, the supernatants were collected to measure the remaining turbidity using a HACH 2100P turbidimeter.

The conditions above for slow mixing were determined based on assessing the hydraulic horizontal flow flocculation at the DWTP. In this assessment, average velocity gradients (G) and flocculation times (t_f) were calculated for the three sections of the flocculation, considering the most frequently used flow rate at the DWTP (30 L s^{-1}). This calculation was done following the methodology outlined by Di Bernardo and Dantas [31]. To calculate G and t_f, the dimensions (width, length, depth, slope, plate-to-plate spacing and plate-to-wall spacing) were determined, and water velocities in each section of the flocculator were measured. The FH950 handheld flow meter (HACH) was employed for velocity measurements. The assessment results for the three sections of the flocculator, along with the respective rotational speeds in the jar test equipment, are provided in Table 1. The rotational speed was determined based on the curves employed to calculate G in the standard jar test apparatus.

2.3. Pilot test for WTS generation

To gather an adequate sample quantity for the characterisation of each WTS type, pilot-scale coagulation, flocculation and sedimentation tests were conducted in a 70 L tank. This tank was equipped with a mechanical mixing system featuring a pitched-blade turbine-type impeller, sampling valves at various depths, and a bottom valve for extracting WTS (Fig. 1). Water sampling for the pilot test was performed using a bucket in the DWTP inlet channel. The samples were immediately carried to the plant laboratory and deposited in the tank. The time elapsed between water sampling and the start of the tests was, at most, 30 min. The pilot tests were executed under similar conditions for the G and t_f conditions, as outlined in Table 1. For this pilot system, the rotational speed was computed using Eq. (1) and Eq. (2) [32].

$$G = \sqrt{\left(\frac{P_w}{\mu \forall}\right)} \tag{1}$$

where G (s^{-1}) represents the average velocity gradient, P_w (W) is the power of the mixing input to water, μ (Pa s) is the dynamic viscosity of water and ∀ (m^3) is the volume of water.

$$n = \left[\frac{P_m}{N_p (D_i)^5 \rho}\right] \tag{2}$$

where n (rpm) represents rotational speed, P_m (W) is the power of the motor, N_p is the (dimensionless) impeller constant or power number, D_i (m) is the impeller diameter and ρ (kg m^{-3}) is the density of water. $N_p = 1.26$ and $D_i = 0.16$ m for the impeller of the pilot system. Furthermore, $P_m = 0.8P_w$ because the efficiency of transferring motor power to water is about 80 % [32]. The rotational speeds necessary to achieve G values of 38, 35 and 23 s^{-1} (Table 1) in the pilot system were 58, 55 and 42 rpm, respectively. Rapid mixing was conducted for 1 min at a G of approximately 200 s^{-1}, and the sedimentation time was 90 min.

Before each pilot test, samples were collected to characterise the raw water. Likewise, after the sedimentation stage, water samples were taken from valves V1–V5 of the pilot system (Fig. 1) to obtain an integrated sample representing the treated water. WTS extraction was conducted through valve V6 (Fig. 1). The volume of WTS extracted from the pilot tank was transferred to two Imhoff

Table 1
G and t_f in flocculator sections.

Flocculator section	t_f (min)	G (s^{-1})	Rotational speed in jar test (rpm)
1	13.0	38	43
2	2.5	35	40
3	4.5	23	30

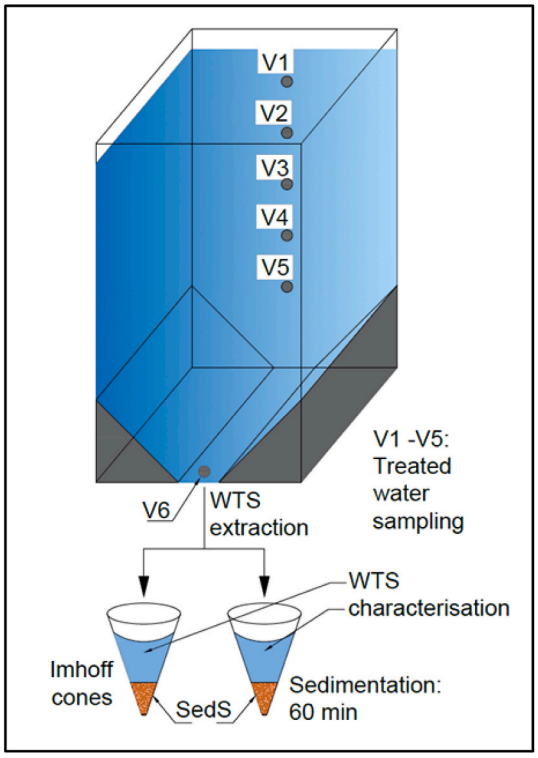

Fig. 1. Scheme of the pilot test system.

cones and left to settle for 60 min. Subsequently, the volume of WTS generated in each pilot test was determined (in mL of WTS per litre of raw water) based on the settleable solids (SedS) measurement. Following the SedS measurement, the WTS samples in the Imhoff cones were mixed, homogenised and stored to measure additional parameters in the WTS. Section 2.4 details the parameters measured in the raw water, treated water and the WTS obtained in the pilot tests.

2.4. Characterisation of WTS, raw water and treated water

To assess the correlations between WTS characteristics, water quality and the drinking water treatment process, the following parameters were analysed for the raw water, treated water and wet WTS samples obtained in the pilot tests: total solids (TS, method: SM-2540-B [33]), total suspended solids (TSS, method: SM-2540-D [33]), aluminium (Al, method: SM-3500-Al B [33]), total iron (Fe: method: SM-3500-Fe B [33]) and pH (HACH HQ40d multiparameter equipment). Furthermore, the wet WTS samples were subjected to TSS and total fixed solids (TFS, SM-2540-E [33]) measurements. Additionally, turbidity (HACH 2100P turbidimeter), electrical conductivity (EC, HACH HQ40d multiparameter equipment), dissolved organic carbon (DOC, ASTM D-7573 [34]) and true colour (SM-2120 C [33]) were measured in the raw and treated water.

Additional characterisations were conducted for all WTS types to gain insights into their physicochemical and surface properties. This information could offer potential pathways for their reuse and valorisation. Thus, the main chemical compounds present in the WTS samples were determined using energy-dispersive X-ray fluorescence (ED-XRF) with the Thermo ARL Optim'X WDXRF. Mineral analysis used an X-ray diffractometer (Malvern PANalytical) with copper (Cu, $K\alpha = 0.15406$ nm) as the radiation source. Measurements covered a 2θ range from 4 to 80° with a 0.05° step. Quantification was done using the HighScore Plus software, employing the Rietveld method and referencing the Inorganic Crystal Structure Database: ICSD FIZ Karlsruhe 2012-1. Fourier transform infrared spectroscopy (FTIR; Spectrum-two, PerkinElmer with UATR) was employed to analyse the active functional groups within the WTS samples across the 4000–450 cm^{-1} range. Particle size analysis of the WTS was conducted using laser diffraction with the Master Sizer 2000E (Malvern PANalytical), equipped with the manual wet sample dispersion unit Hydro 2000MU. The solids addition method determined the zero-charge point pH (pH_{PZC}; [35]). The hydrochloric acid (HCl) and sodium hydroxide (NaOH) used in pH_{PZC} tests were obtained from Merck S.A. (Germany).

2.5. Estimation of WTS production

The quantity of dry WTS produced during the pilot test (m_{cal}) was estimated using the equations presented by Kawamura [36], Vianna et al. [37] and AWWA and Edzwald [38]. These equations replaced the flow rate (Q) with volume (V) to align them with the pilot system's operational conditions, which operate in batch mode. Furthermore, the equation introduced by Kawamura was

converted to the International Unit System.

Kawamura [36]:

$$m_{calc} = V(1.30Tu_{RW} + 0.26D_{alum})10^{-3} \quad (3)$$

Vianna et al. [37]:

$$m_{calc} = V(0.75Tu_{RW} + 0.44D_{alum})10^{-3} \quad (4)$$

AWWA and Edzwald [38]:

$$m_{calc} = V(0.44D_{alum} + DOC_r + TSS + A)10^{-3} \quad (5)$$

where m_{calc} = WTS production calculated (g), V = volume of raw water in the pilot tank (L), Tu_{RW} = raw water turbidity (NTU), D_{alum} = alum doses as 17.1 % of Al_2O_3 (mg L^{-1}), DOC_r = DOC removed (mg L^{-1}), TSS = raw water total suspended solids (mg L^{-1}) and A = additional chemicals added such as polymer or clay (mg L^{-1}).

Eq. (3) is based on the following chemical reaction (Eq. (6)), and the factor 0.26 in this equation is the mass ratio between the aluminium hydroxide produced and the alum dosed:

$$Al_2(SO_4)_3 \bullet 14H_2O + 3Ca(HCO_3)_2 \rightarrow 3CaSO_4 + 2Al(OH)_{3(s)} + 6CO_2 + 14H_2O \quad (6)$$

Eq. (4) and Eq. (5) assume that three waters of hydration are chemically bound to aluminium hydroxide, as shown chemical reaction in Eq. (7). Therefore, the mass ratio between aluminium hydroxide produced and alum is equal to 0.44 in both equations (2Al$(OH)_3$3H_2O(s)/$Al_2(SO_4)_3$14H_2O)

$$Al_2(SO_4)_3 \bullet 14H_2O + 6HCO_3^- \rightleftharpoons 2Al(OH)_3 \bullet 3H_2O_{(s)} + 6CO_2 + 8H_2O + 3SO_4^{2-} \quad (7)$$

The estimation error in WTS production was calculated by comparing the WTS production values obtained from each equation (m_{cal}) with the experimental WTS production values (m_{exp}), as shown in Eq. (8). m_{exp} values were determined based on the TS measurements in the WTS samples collected during the pilot tests.

$$E = \frac{(m_{calc} - m_{exp})}{m_{exp}} 100 \quad (8)$$

where E = estimation error in the WTS production (%), m_{calc} = WTS production calculated (g) and m_{exp} = WTS production measured (g).

3. Results and discussion

3.1. Operative conditions of DWTP

Fig. 2 shows the monthly mean, minimum and maximum values of raw water turbidity (Tu_{RW}) at the DWTP and the monthly rainfall data from 2016 to 2020. During this period, the average Tu_{RW} values ranged from 1.4 to 27.3 NTU, with maximum values reaching 870 NTU. The months exhibiting significant increases in average and maximum Tu_{RW} values correlate with the rainfall

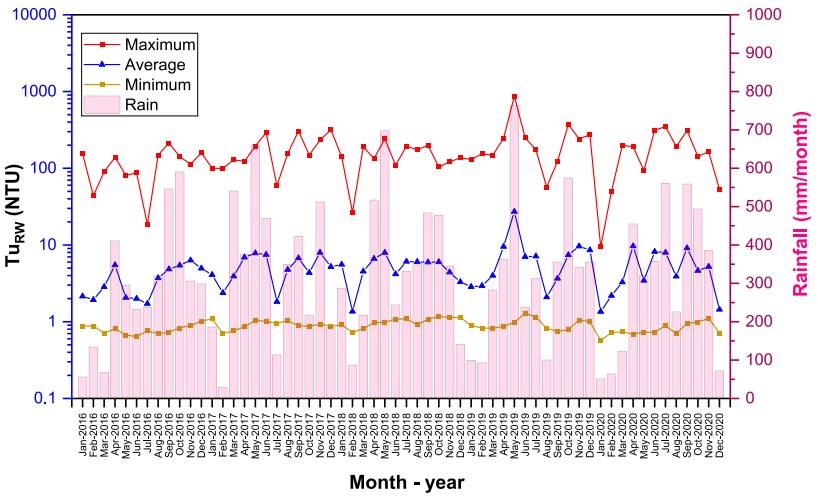

Fig. 2. Raw water turbidity data for the DWTP and rainfall data for 2016–2020.

patterns, as Lee et al. [39] reported.

The 90th percentiles (P_{90}) for monthly Tu_{RW} at the DWTP were calculated and grouped by month (Fig. 3). These P_{90} values were used to define the following categories for the raw water characteristics: low turbidity ($P_{90} < 5$ NTU), medium turbidity ($5 \leq P_{90} < 10$ NTU) and high turbidity ($P_{90} \geq 10$ NTU). As depicted in Fig. 3, P_{90} values for Tu_{RW} were less than 5 NTU during 32 of the 60 months in the data analysis period. Consequently, the low turbidity category was predominant in the evaluated DWTP, with the medium turbidity category following closely behind. During the experimental period at the DWTP, an exceptionally high raw water turbidity occurred (Tu_{RW} around 300 NTU). Therefore, it was decided to introduce a fourth category of raw water, referred to as very high turbidity. The operational records of the DWTP indicated that the coagulant doses applied to raw water in alignment with each turbidity category were as follows: low turbidity (4–6 mg alum L^{-1}), medium turbidity (6–8 mg alum L^{-1}), high turbidity (8–10 mg alum L^{-1}) and very high turbidity (16–20 mg alum L^{-1}). Consequently, jar tests were performed to verify the efficacy of these coagulant doses in a wider range, and the findings are detailed in the subsequent section.

3.2. Jar test results

The outcomes of turbidity removal and the resulting treated water turbidity (Tu_{TW}) from the jar tests conducted with various coagulant doses (low, medium and high turbidity: 4–10 mg alum L^{-1} and very high turbidity: 14–24 mg alum L^{-1}) for each type of raw water are depicted in Fig. 4a–d. When using low-turbidity raw water (Fig. 4a), the lowest turbidity removal (37 %) was observed when comparing the results of the optimal doses. The optimal dose for this type of water was 4 mg alum L^{-1}, resulting in a Tu_{TW} of 1.6 NTU. Additionally, by using the optimal doses in the tests with medium (6 mg alum L^{-1}) and high (8 mg alum L^{-1}) turbidity raw water (Fig. 4b and c, respectively), similar Tu_{TW} values (~2.4 NTU) were attained, resulting in 66 % and 91 % turbidity removal, respectively. Finally, Fig. 4d illustrates that the highest turbidity removal (99.8 %) and the lowest Tu_{TW} of 0.72 NTU were achieved with very high turbidity raw water using an optimal coagulant dose of 16 mg alum L^{-1}. This Tu_{TW} value is below the World Health Organization's (WHO's) recommended limit of 1.0 NTU for effective disinfection [40], even without a filtration stage. Table 2 summarises the optimal coagulant doses for each raw water category utilised in the pilot tests to evaluate WTS characteristics.

3.3. Characterisation of wet WTS, raw water and treated water

Fig. 5 presents the results obtained for turbidity and EC of raw and treated water in the pilot tests conducted using the optimal coagulant dosage for each water type or category obtained in Section 3.2 and reported in Table 2. As shown in Fig. 5a, despite significant differences in the turbidity levels of the raw water across the various types of water evaluated, the treated water exhibited similar values, ranging from 0.83 to 3.28 NTU. Consequently, the very-high-turbidity water demonstrated the most substantial reduction in turbidity reaching a turbidity of 0.89 NTU in the treated water complying with the recommendations of the WHO Guidelines for Drinking-Water Quality, which also implies a greater removal of TSS that accumulate in the WTS. In all four types of water, an increase in the EC of the treated water was observed when compared to the raw water, as illustrated in Fig. 5b. This outcome is attributed to the contribution of ions through the dissociation of the coagulant, which increases EC, as reported by Gandiwa et al. [41].

NOM is a mixture of organic compounds detected in surface waters, which is measured as DOC or total organic carbon. True colour measurement can also represent the residual NOM in water [42]. Fig. 6 shows that the types of raw water with the highest turbidity levels (VH and H) also exhibit elevated levels of NOM, as indicated by DOC concentrations ranging from 4.51 to 4.65 mg L^{-1} (Fig. 6a) and true colour levels between 23.6 and 29.3 CU (Fig. 6b). In the pilot test with low-turbidity water (L), the raw and treated water samples displayed the lowest levels of NOM. The DOC and true colour measurements in both samples were below the quantification limit of their respective analytical methods (1.0 mg L^{-1} for DOC and 5.0 CU for true colour). Water types M, H and VH exhibited DOC removal rates ranging from 36.7 % to 65.2 %. As the trend observed with turbidity, the treatment of VH-type water resulted in the

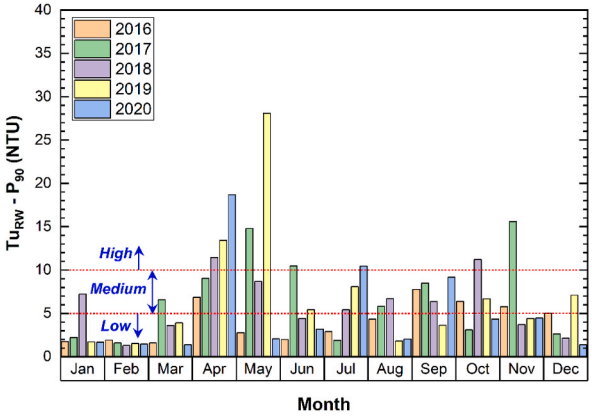

Fig. 3. P_{90} for raw water turbidity data.

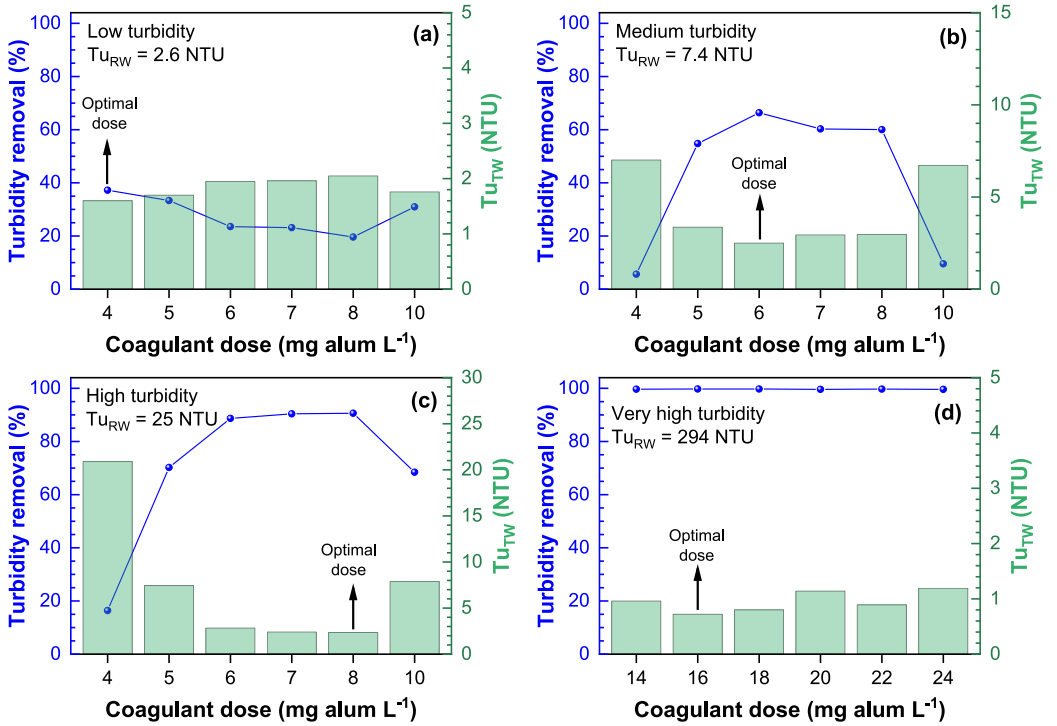

Fig. 4. Turbidity removal and Tu_{RW} in jar tests: (a) Low turbidity; (b) Medium turbidity; (c) High turbidity; (d) Very high turbidity.

Table 2
Results for optimal coagulant dose tests.

Raw water category	Turbidity range (NTU)	Turbidity in raw water samples - Tu_{RW} (NTU)	Coagulant dose (mg alum L^{-1})	Turbidity in treated water samples - Tu_{TW} (NTU)	Turbidity removal (%)
Low turbidity (L)	<5	2.6	4	1.6	38.5
Medium turbidity (M)	5–10	7.4	6	2.5	66.2
High turbidity (H)	10–30	25	8	2.3	90.8
Very high turbidity (VH)	~300	294	16	0.72	99.8

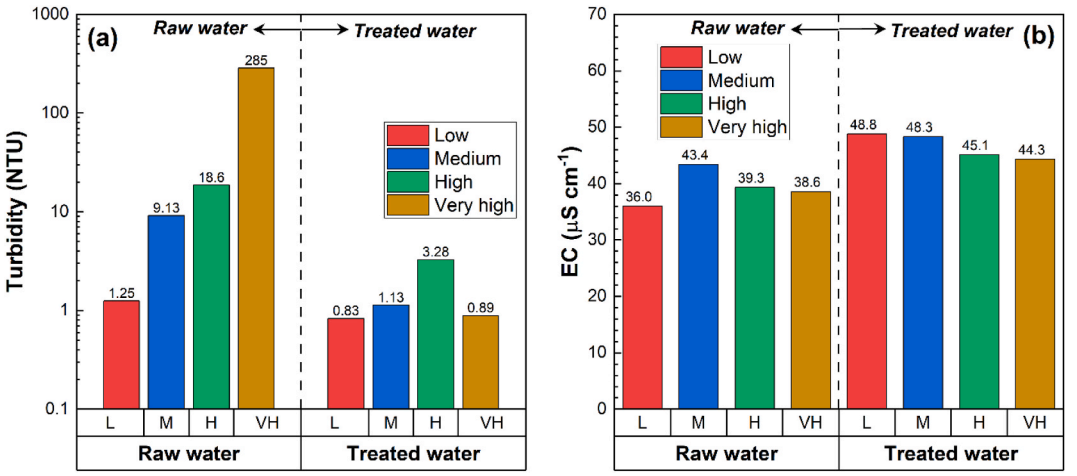

Fig. 5. Results for raw water (left side) and treated water (right side) in pilot tests: (a) Turbidity; (b) EC.

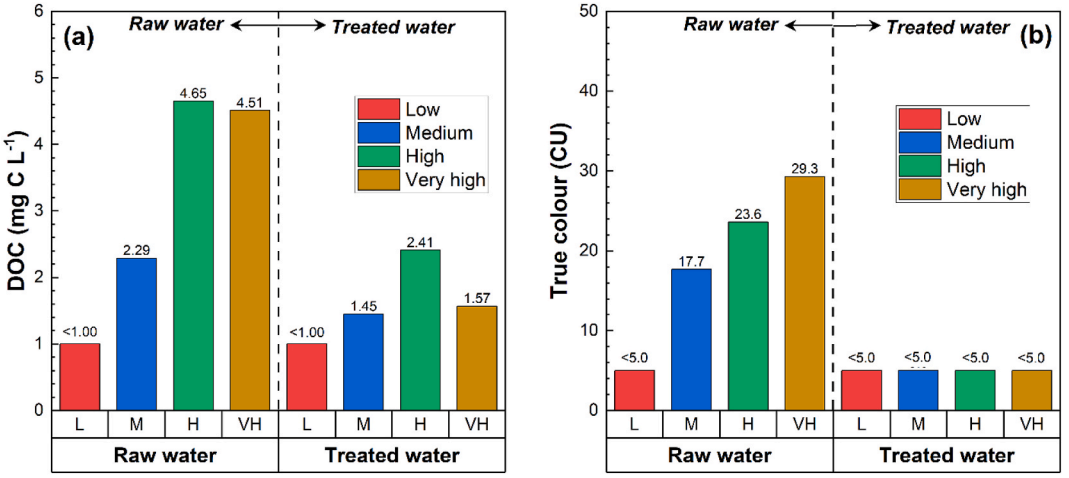

Fig. 6. Results for raw water (left side) and treated water (right side) in pilot tests: (a) DOC; (b) True Colour.

highest DOC removal of 2.94 mg L^{-1} (DOC_r). NOM can be absorbed by aluminium hydroxide precipitates formed in coagulation-flocculation stages and then removed by flocs sedimentation [43]. NOM removal also contributes to the accumulation of solids in the water treatment system [44].

Figs. 7–9 depict the outcomes concerning solids (TS and TSS), metals (aluminium (Al) and total iron (Fe)) and pH values for the wet sludge, raw water and treated water. The WTS is designated based on the raw water type from which they were generated, as follows: low-turbidity WTS (L-WTS), medium-turbidity WTS (M-WTS), high-turbidity WTS (H-WTS) and very-high-turbidity WTS (VH-WTS).

In Fig. 7, a consistent and increasing pattern in the mass of TS (Fig. 7a) and TSS (Fig. 7b) was observed across the various types of generated WTS. The L-WTS exhibited the lowest solids mass (TS = 155 mg and TSS = 91 mg), with mass progressively increasing in the following order: L-WTS < M-WTS < H-WTS < VH-WTS. This trend can be attributed to the increase in alum dosing as the turbidity of the raw water rises (Table 2). This, in turn, leads to a higher production of aluminium hydroxide (Eq. (6) – (7)), a component of the WTS. Additionally, the accumulation of removed solids (difference between the solids in raw water and treated water) in the WTS also rises with increasing turbidity of the raw water, as shown in Fig. 7. The VH-WTS displayed significantly elevated solid contents, surpassing the mass of TS obtained for the L-WTS by over 130 times and exceeding the mass of TSS by over 200 times. This finding confirms the influence of the raw water quality, the coagulant doses applied during treatment and the treatment efficiency on the mass of WTS generated at the DWTP, as reported by Gregory and Dillon [45].

The results for Al and Fe are depicted in Fig. 8a and b, respectively. The presence of both elements was detected in all types of raw water assessed, with iron showing a higher content. Al can exist in soluble or colloidal forms in raw water, often as a component of aluminosilicate-type clays [46]. Furthermore, it is widely acknowledged that iron oxides are prevalent in natural environments and aquatic systems, with Fe-rich particles being recognised as ubiquitous components for decades [47]. In Fig. 8a, it is evident that a fraction of the alum dosed in type L, M and H waters remains in the treated water (12–16 mg Al, equivalent to concentrations of 0.177–0.228 mg Al L^{-1}), either in soluble form or as part of particles that are not removed during the treatment process. The use of

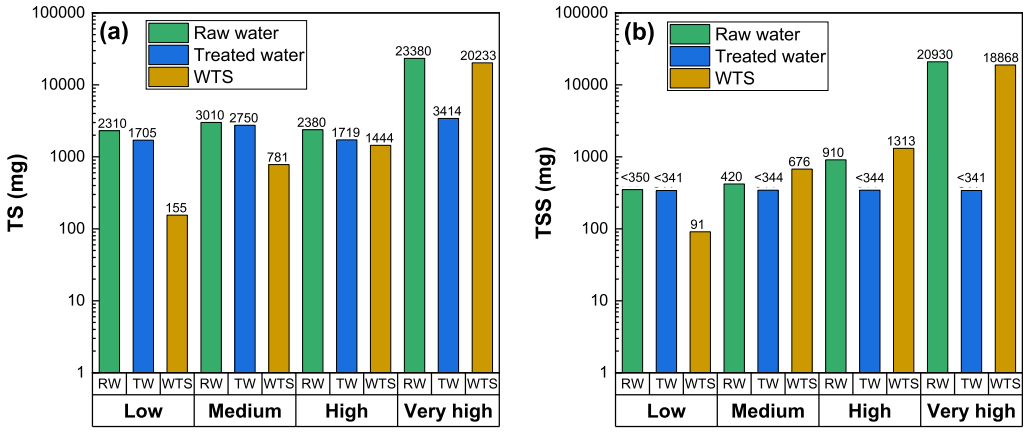

Fig. 7. Results for wet WTS, raw water and treated water: (a) TS; (b) TSS.

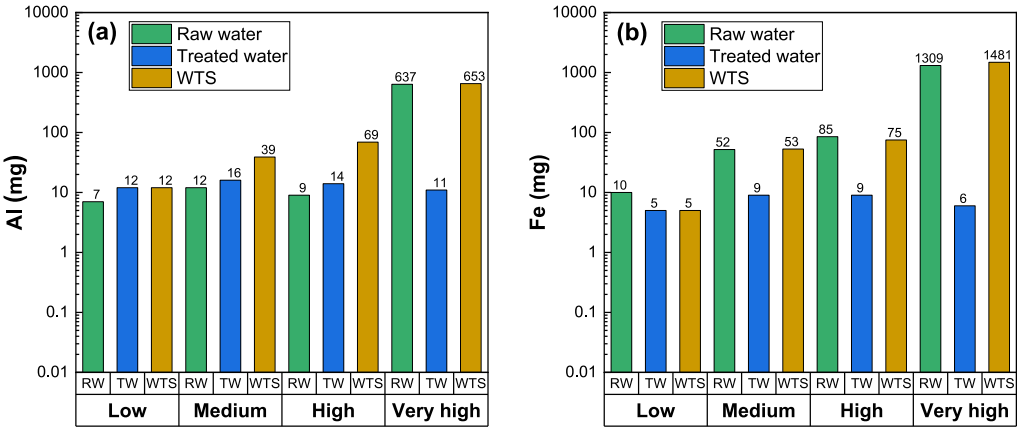

Fig. 8. Results for wet WTS, raw water and treated water: (a) Al; (b) Fe.

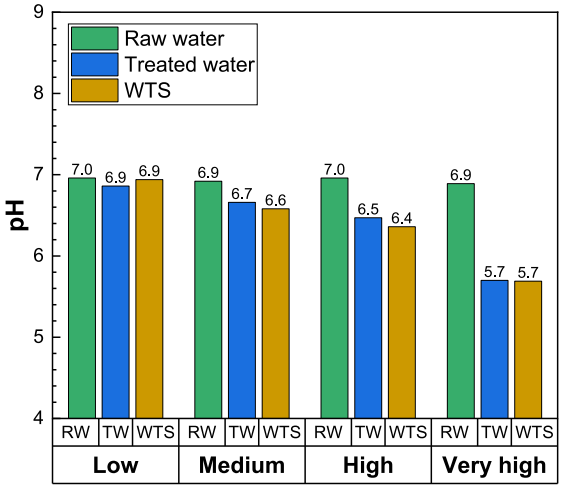

Fig. 9. pH for wet WTS, raw water and treated water in pilot tests.

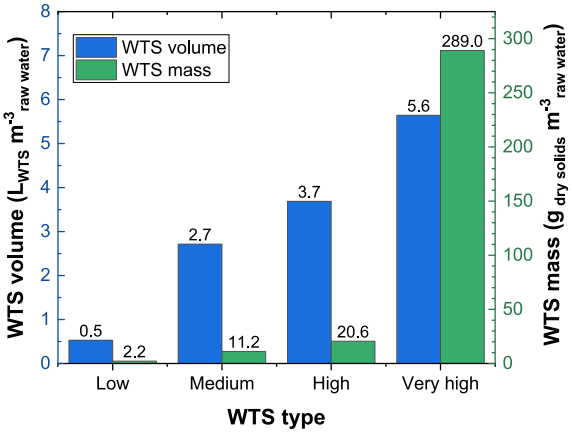

Fig. 10. Volume and mass of WTS produced.

lower coagulant doses in treating these types of raw water can cause the residual aluminium remaining in the treated water [48]. In contrast, the lowest amount of residual aluminium (11 mg, equivalent to a concentration of 0.166 mg Al L^{-1}) was observed for VH-WTS despite applying the highest alum dose. This result indicates a more effective coagulation process for VH-WTS. As shown in Fig. 8b, all types of water exhibited lower iron levels in the treated water compared to their respective raw water, signifying substantial reductions in iron mass through coagulation and particle sedimentation effects, ranging from 51.6 % to 99.5 %.

Fig. 8 shows that the Al and Fe content in the WTS follows a similar trend as analysed for TS and TSS. L-WTS shows the lowest mass of Al and Fe (12 mg of Al and 5 mg of Fe), with mass progressively increasing as follows: M-WTS (39 mg of Al and 53 mg of Fe), H-WTS (69 mg of Al and 75 mg of Fe) until reaching its maximum values in the VH-WTS (653 mg of Al and 1481 mg of Fe). The Al and Fe content in the four types of WTS analysed indicates their potential for coagulant recovery.

The pH was consistent across all the raw waters studied, with reported values ranging from 6.9 to 7.0 (Fig. 9). Upon the addition of alum, which reacts with the water's alkalinity (Eq. (6) and Eq. (7)), a decrease in the pH values of the treated water occurred (from 6.9 to 5.7), with a more pronounced drop associated with higher alum doses. The pH values observed in the WTS were similar to those in the corresponding treated water. Therefore, WTS types L, M and H displayed pH values ranging from 6.9 to 6.4, while VH-WTS recorded the lowest pH value (5.7) because of the higher alum dose used in treating the water that produced this WTS type. All the reported pH values fall within the typical range documented for alum sludges (5.12–8.0), according to Turner et al. [49].

The production of WTS per unit of treated water is presented in Fig. 10. The volume and mass of the WTS were calculated from settleable solids (SedS) and TS, respectively. As depicted in Fig. 10, the volume of WTS produced increased with the rising turbidity of the raw water. Consequently, the lowest volume of WTS production was associated with the L-WTS (0.5 L_{WTS} $m^{-3}_{raw\ water}$), while the highest volume was observed in the VH-WTS t (5.6 L_{WTS} $m^{-3}_{raw\ water}$). These findings indicate that between 0.05 % and 0.56 % of the volume treated in the coagulation, flocculation and sedimentation stages of the DWTP becomes wastes represented by WTS. The generated mass of WTS exhibits a similar trend as the volume, with a minimum value of 2.2 g $_{dry\ solids}$ $m^{-3}_{raw\ water}$ for the L-WTS and a maximum of 289 g $_{dry\ solids}$ $m^{-3}_{raw\ water}$ for the VH-WTS. Considering the average flow rate of the DWTP influent reported for the year 2020 (24 L s^{-1}), during months of low raw water turbidity, approximately 31 m^3 or 137 kg $_{dry\ solids}$ per month of WTS can be generated, while in months of high turbidity, approximately 230 m^3 or 1281 kg $_{dry\ solids}$ per month of WTS may be produced. Notably, during an extreme event of raw water turbidity, approaching the evaluated very high turbidity value of 285 NTU, it is possible to generate approximately 1.0 m^3 or 50 kg $_{dry\ solids}$ of WTS in the DWTP within just 2 h of treatment with the average flow rate.

In Fig. 11, it is evident that all types of evaluated WTS consistently exhibited values greater than 0.5 for the TSS/TS and TFS/TS solids ratios. These findings imply that across all WTS types, TSS are more dominant than total dissolved solids. Likewise, TFS predominate over the total volatile solids, indicating that a significant portion of the WTS is inorganic in nature, as reporting Ahmad et al. [28]. Notably, the L-WTS exhibited the lowest TSS/TS value (0.59), which can be attributed to the fact that the treatment process for the water responsible for generating this sludge resulted in the lowest removal of turbidity (as shown in Fig. 5a) and TSS (as depicted in Fig. 7b). In contrast, the M-WTS and H-WTS types displayed the lowest TFS/TS values (ranging from 0.57 to 0.67), indicating a higher proportion of volatile solids within these WTS samples, which include the organic matter removed during the treatment process.

3.4. Characterisation of dry WTS

The chemical composition and mineral phases of the WTS are presented in Fig. 12. The primary components of all WTS in terms of oxides include Al_2O_3 (29.9–33.9 %), SiO_2 (20.5–26.4 %) and Fe_2O_3 (11.3–12.9 %). The X-ray diffraction results suggest that all WTS samples are predominantly amorphous, constituting 45.1–65.2 %, with the presence of crystalline structures such as aluminium–silicate clays (kaolinite 1A, illite 2M1, and dickite 2M1), quartz and low magnetite. These minerals include the main elements

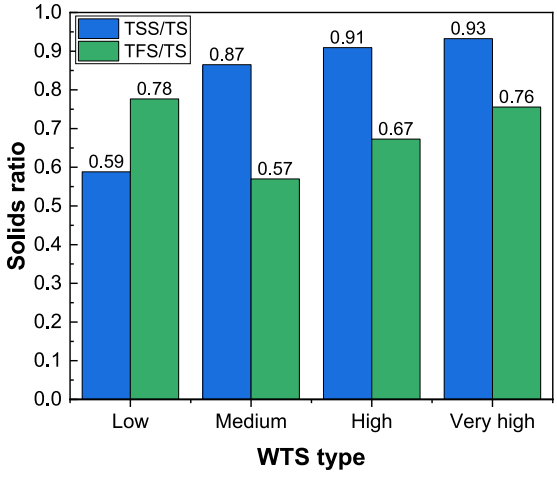

Fig. 11. TSS/TS and TFS/TS solids ratios in WTS.

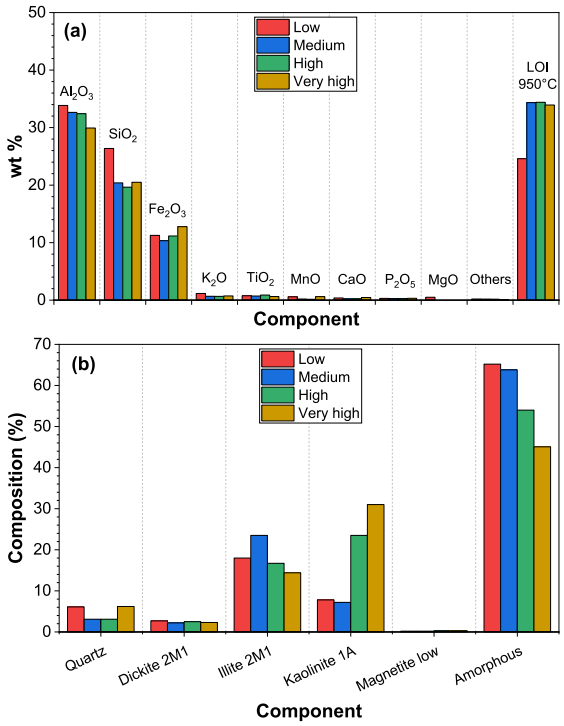

Fig. 12. Composition of WTS: (a) Chemical composition; (b) Mineral phases.

(Al, Si and Fe) identified in the XRF analysis. Additionally, amorphous material can include Fe and Al as $Fe(OH)_3$ and $Al(OH)_3$ formed during coagulation-flocculation stages [50,51]. The loss of ignition (LOI) at 950 °C in WTS is linked to the content of organic matter and minerals that undergo dehydroxylation processes during calcination, such as kaolinite, illite and dickite [52–54]. As shown in Fig. 12b, WTS of types M, H and VH displayed similar values of LOI at 950 °C within the range of 33.9 %–34.4 %, whereas L-WTS exhibited a lower LOI at 950 °C of 24.6 %. This reduced LOI at 950 °C value in L-WTS can be attributed to its lower content of aluminium–silicate clays (28.5 %) and organic matter, as evidenced by its high TFS/TS ratio (0.78) reported in Fig. 11.

The high content of aluminium (Al) and iron (Fe) reported in the four types of WTS studied, both in their wet state (Fig. 8) and dry state (Fig. 12a), renders them potential coagulants for application in wastewater treatment. This application can be achieved directly using unmodified or chemically modified WTS [55,56]. Additionally, coagulants can be recovered from WTS through various physicochemical techniques [18] for subsequent use in wastewater treatment [7,57–59]. According to the study by Nair and Ahammed [27], a higher percentage of coagulant can be recovered from L-WTS by acidification, as this type of sludge is generated from raw water with the lowest levels of turbidity and organic matter (Figs. 5a and 6a).

Fig. 13 and Table 3 depict the particle size distribution in the WTS. In Fig. 13, it is evident that the L-WTS and M-WTS exhibit similar particle distributions, with D_{90} values close to 150 μm (Table 3). On the other hand, WTS types H and VH show smaller particle sizes, with D_{90} values of 116.5 μm and 86.6 μm, respectively. Table 3 provides further details, indicating that all WTS samples contain less than 40 % of particle volume in the sand range (75 μm $\leq$ dp $<$ 4.75 mm) and increased volumes (61.0–85.9 %) of particles in the fines range (dp $<$ 75 μm), as defined by ASTM [60]. The content of sand in the four WTS is lower than the values reported by Dassanayake et al. [43] for alum sludges (60.4–69.0 %). The particles in the fines range of WTS encompass silts, clays (as identified in Fig. 12b) and organic matter, a component of the amorphous material that contributes to the LOI at 950 °C (Fig. 12a).

The zero-charge point pH (pH_{PZC}) is the pH at which the net surface charge on the WTS surface becomes neutral, with the positive and negative charges of the material equal [61]. The pH_{PZC} is a crucial parameter that influences the use of WTS as adsorbents or coagulants for contaminants removal in aqueous solutions [8]. Fig. 14 shows that WTS types L, M and H exhibit pH_{PZC} values in the range of 6.4 and 6.6, whereas VH-WTS has a lower pH_{PZC} of 5.7. These pH_{PZC} values align closely with the corresponding pH values of wet WTS and treated water (Fig. 9). When the solution pH is lower than the pH_{PZC}, the WTS surface will be positively charged and interact with negative species. Conversely, if the solution pH is higher than the pH_{PZC} of the WTS, the surface becomes negatively charged and will interact with positively charged pollutants [62]. Hence, for aqueous solutions with a pH less than 5.7, all WTS exhibit strong potential for adsorbing pollutants such as metals (Pb^{+2}, Cu^{+2}, Cd^{+2}) and cationic dyes. In contrast, for pH values exceeding 6.6, WTS can be advantageous in removing contaminants like anionic dyes and phosphates [7].

The functional groups of WTS analysed by ATR-FTIR are illustrated in Fig. 15. The band observed in the 3020 to 3780 cm^{-1} range in L-WTS is attributed to the OH stretch of sorbed water and mineral hydroxide phases [63,64]. The slight increase in the intensity of this band observed in WTS types M, H and VH can be attributed to a higher content of aluminium–silicate clays and water. NOM is

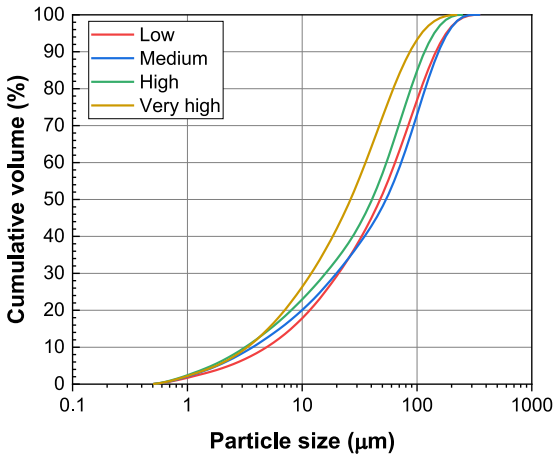

Fig. 13. Particle size distribution in WTS.

Table 3
Particle size analysis in WTS.

WTS type	D_{90} (µm)	Fines (clays, silts) $d_p < 75$ µm (% volume)	Sands 75 µm $\leq d_p <$ 4.75 mm (% volume)
Low (L)	146.0	65.6	34.4
Medium (M)	153.8	61.0	39.0
High (H)	116.5	73.2	26.8
Very high (VH)	86.6	85.9	14.1

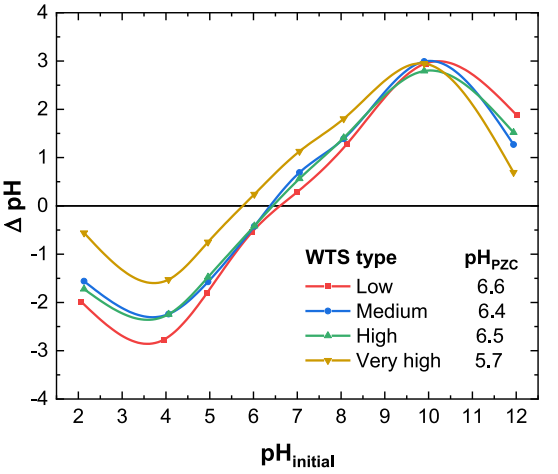

Fig. 14. pH_{PZC} of WTS.

associated with bands around 1640 cm^{-1} (C=C, C=O) and 1400 cm^{-1} (COO-, C-O) in all WTS [63,65]. These bands exhibit similar intensity in L-WTS and VH-WTS. They increase for M-WTS and H-WTS due to the higher content of organic matter in these latter two WTS types, as indicated by the lower ratios of TFS/TS in Fig. 11. Bands attributed to the silica network fall within the range of 465–1150 cm^{-1} [66], corresponding to the structures of quartz and the clays identified in the XRD analysis. Peaks at approximately 1030 cm^{-1} and 465 cm^{-1} are linked to Si–O vibrations, as indicated by Shamaki et al. [64]. Moreover, the band at 914 cm^{-1} is associated with the elongation of Al–OH bonds [62], and the Fe–O vibrations of Fe_2O_3 can be observed at 534 and 522 cm^{-1} [26]. All the previously mentioned bands in the range of 465–1030 cm^{-1} exhibited an increase in intensity in the VH-WTS, which can be attributed to its higher content of mineral phases, as shown in Fig. 12b.

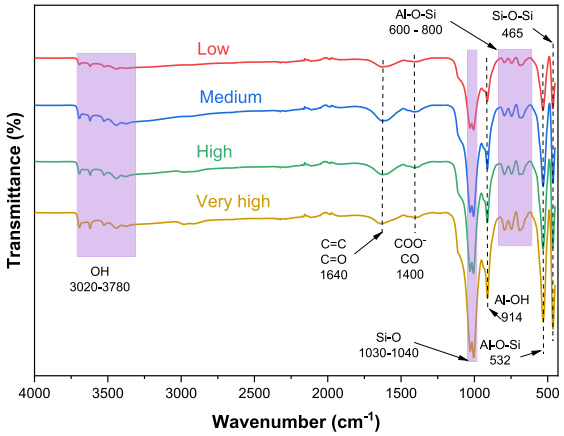

Fig. 15. FTIR spectra of WTS.

3.5. WTS production estimation

Table 4 summarises the results of the variables used in Eq. (3) [36], Eq. (4) [37], and Eq. (5) [38] for estimating the quantity of dry WTS produced during the pilot tests. The experimental WTS production (m_{exp}), calculated production (m_{cal}), the error (calculated by Eq. (8)), the coefficient of determination (R^2) and the root mean square error (RMSE) are presented in Table 5.

The errors obtained with Eq. (3) indicate an overestimation ranging from 20 % to 30 % in the production of all types of sludge with this model. The model corresponding to Eq. (4) showed an overestimation in the generation of L-WTS (21.8 %) and underestimates in the 15 %–23.6 % range for producing other types of WTS. Eq. (5) presents errors of less than |10 %| in the production of WTS types H and VH but also exhibits the greatest overestimation (>200 %) in the quantity produced of L-WTS. The three models evaluated presented high values for the R^2 (>0.999); however, none of them provided a good fit in estimating WTS production for all types of WTS due to the high overestimation and underestimated errors obtained and RMSE values reported (0.7232–3.0076). Therefore, some modifications were made to the original equations, resulting in Eqs. (9)–(11).

$$m_{calc} = V\left(\left(R_{TSS/Tu} \times Tu_{RW}\right) + 0.26D_{alum}\right)10^{-3} \quad (9)$$

$$m_{calc} = V\left(\left(R_{TSS/Tu} \times Tu_{RW}\right) + 0.44D_{alum}\right)10^{-3} \quad (10)$$

$$m_{calc} = V\left(0.44D_{alum} + DOC_r + \left(R_{TSS/Tu} \times Tu_{RW}\right) + A\right)10^{-3} \quad (11)$$

where m_{calc} = WTS production calculated (g), V = volume of raw water in the pilot tank (L), Tu_{RW} = raw water turbidity (NTU), $R_{TSS/Turbidity}$ = correlation coefficient between TSS and Tu_{RW} (1.01), D_{alum} = alum doses as 17.1 % de Al_2O_3 (mg L^{-1}), DOC_r = DOC removed (mg L^{-1}) and A = additional chemicals added such as polymer or clay (mg L^{-1}).

As recommended by Kawamura [36] and AWWA and Edzwald [38], the correlation coefficient between TSS and turbidity (RTSS/turbidity) for the DWTP was calculated based on simultaneous measurements of TSS and turbidity in multiple raw water samples, as illustrated in Fig. 16. This correlation coefficient replaced the values 1.3 and 0.75 in Eq. (3) and Eq. (4), resulting in Eq. (9) and Eq. (10), respectively. Additionally, the TSS (measured) in Eq. (5) was substituted by the factor $R_{TSS/Turbidity}$ Tu_{RW}, representing the TSS calculated through the equation presented in Fig. 16, resulting in Eq. (11). The value of the correlation coefficient ($R_{TSS/Turbidity}$) obtained (1.01) falls within the ranges reported by Kawamura [36]; between 1.0 and 2.0 and AWWA and Edzwald [38]; between 0.7 and 2.2.

Table 6 presents the results for WTS production calculated using Eq. (9), Eq. (10) and Eq. (11), including model coefficients and the

Table 4
Parameters for estimating WTS production.

WTS type	D_{alum} (mg L^{-1})	Raw water			Treated water	DOC_r (mg L^{-1})
		Tu_{RW} (NTU)	TSS (mg L^{-1})	DOC (mg L^{-1})	DOC (mg L^{-1})	
Low (L)	4	1.25	<5	<1.00	<1.00	0[a]
Medium (M)	6	9.13	6	2.29	1.45	0.84
High (H)	8	18.6	13	4.65	2.41	2.24
Very high (VH)	16	285	299	4.51	1.57	2.94

Note.
[a] Assuming DOC = 1.0 mg L^{-1} (method quantification limit – MQL) for raw and treated water.

Table 5
WTS production estimating by Eqs. (3)–(5).

WTS type	m_{exp} (g)	Eq. (3)		Eq. (4)		Eq. (5)	
		m_{calc} (g)	E (%)	m_{calc} (g)	E (%)	m_{calc} (g)	E (%)
Low (L)	0.155	0.187	20.4	0.189	21.8	0.473[a]	205.3
Medium (M)	0.781	0.940	20.4	0.664	−15.0	0.664	−15.0
High (H)	1.444	1.838	27.3	1.223	−15.3	1.313	−9.1
Very high (VH)	20.23	26.23	29.6	15.46	−23.6	21.63	6.9
R^2		1.0000		1.0000		0.9994	
RSME		**3.0076**		**2.4033**		**0.7232**	

Note.
[a] Assuming TSS = 5 mg L^{-1} (method quantification limit – MQL) for raw water.

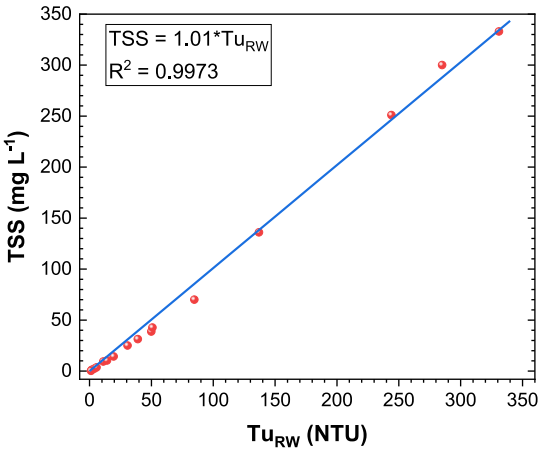

Fig. 16. Correlation between raw water turbidity and TSS.

Akaike Information Criterion (AIC). The values of WTS production calculated with Eq. (9) closely matched the experimental values, with errors less than |5 %|. Furthermore, the high R^2 (1.0000), the lower RSME (0.1062) and the lower AIC (−3.4851) reporting for Eq. (9) show that the Kawamura model adjusted with RTSS/turbidity is the simplest model that presents a better fit to the experimental data. For models corresponding to Eq. (10) and Eq. (11), the estimation was improved, reporting RSME values of 0.2165 and 0.1985, respectively; however, for L-WTS, overestimations close to 37 % were still observed. These findings highlight the importance of knowing the correlation coefficient between TSS and turbidity to accurately estimate WTS production [28]. Furthermore, the best fit of the Kawamura model adjusted with RTSS/turbidity suggests that the chemical reaction presented in Eq. (6) more accurately represents the coagulation process in the studied DWTP. Therefore, this process does not correspond to enhanced coagulation [36].

Fig. 17 illustrates that in Eq. (9), the factor that contributes the most to sludge production is the one associated with turbidity ($R_{TSS/Tu}$ x Tu_{RW}) in the WTS types M, H and VH (77.7–97.6 %). This is because these types of WTS exhibit high TSS removal (Fig. 7b). In contrast, in the generation of WTS type L, there was low TSS removal (Fig. 7b), and the factor related to the coagulant dose and the production of aluminium hydroxide (0.26Dalum) was the most significant (58.2 %).

Table 6
WTS production estimating by Eqs. (9)–(11).

WTS type	m_{exp} (g)	Eq. (9)		Eq. (10)		Eq. (11)	
		m_{calc} (g)	E (%)	m_{calc} (g)	E (%)	m_{calc} (g)	E (%)
Low (L)	0.155	0.161	4.0	0.212	36.5	0.212	36.8
Medium (M)	0.781	0.755	−3.4	0.830	6.3	0.889	14.0
High (H)	1.444	1.461	1.2	1.561	8.1	1.718	19.3
Very high (VH)	20.23	20.44	1.0	20.64	2.0	20.49	3.1
R^2		1.0000		1.0000		0.9999	
RSME		**0.1062**		**0.2165**		**0.1985**	
Model coefficients		**2**		**2**		**3**	
AIC		**−3.4851**		**−2.0606**		**−1.7341**	

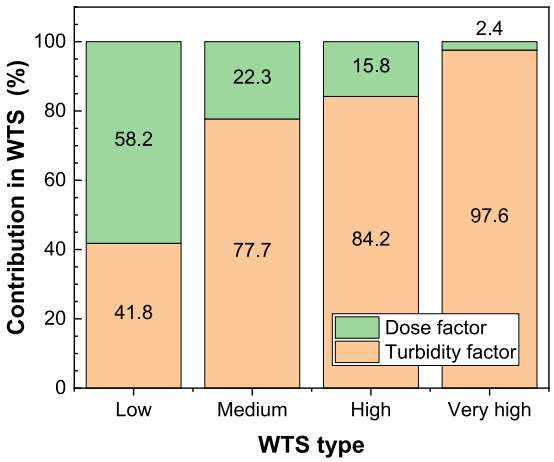

Fig. 17. Contribution in WTS production by factors turbidity and dose in Eq. (9).

4. Conclusions

The analysis of operational condition records at the DWTP over five years revealed significant variability in the turbidity of the raw water, which is linked to rainfall patterns. Among the four types of raw water defined through data analysis and jar tests, the low turbidity (L) category was the most frequently occurring at the DWTP during the study period.

Rainfall seasonality significantly affects WTS production, showing that the smallest amount of sludge was generated with type L raw water (137 kg of dry solids per month for the average flow rate of the DWTP) whereas, in one month, with the average turbidity of raw water in the high turbidity range, WTS generation increase more than nine folds.

The WTS production estimation model proposed by Kawamura, adjusted with the correlation coefficient between raw water turbidity and TSS calculated for the DWTP, demonstrated a good fit for the experimental production data for all types of WTS ($R^2 = 1.0$, RMSE = 0.1062 and the lower Akaike Information Criterion). Therefore, sludge production projections, which are an essential aspect for properly managing WTS, can be made based on the raw water's coagulant dose and turbidity. These two variables are easily and frequently measured in the DWTP.

As a result of its high content of Al (Al_2O_3: 30–34 %) and Fe (Fe_2O_3: 11–13 %), the WTS generated in the studied DWTP have the potential for direct use as coagulants or for the recovery of coagulants that can be used in wastewater treatment. This particularly applies to L-WTS, which is produced from raw water and characterised by low concentrations of NOM and turbidity. Moreover, all the evaluated sludges are primarily amorphous materials, with the presence of some mineral phases, notably kaolinite, illite and dickite. These minerals are more prevalent in VH-WTS, resulting in a higher content of particles in the fine size range for this type of WTS. The presence of aluminium–silicate clays and the functional groups of the silica network observed in the FTIR analysis suggest that WTS, particularly VH-WTS, also have the potential to serve as raw materials for the generation of contaminant adsorbents in aqueous systems. The potential applications of WTS in coagulation and adsorption during wastewater treatment can contribute to the circular economy in the water sector. However, these applications depend on the physical and chemical characteristics of the WTS that are controlled by rainfall seasonality.

Data availability statement

Data will be made available on request.

CRediT authorship contribution statement

Camilo C. Castro-Jiménez: Writing – original draft, Visualization, Methodology, Investigation, Data curation, Conceptualization. **Julio C. Saldarriaga-Molina:** Writing – review & editing, Supervision, Methodology, Conceptualization. **Edwin F. García:** Writing – review & editing, Visualization, Supervision, Methodology, Conceptualization.

Declaration of competing interest

The authors declare that they have no known competing financial interests or personal relationships that could have appeared to influence the work reported in this paper.

References

[1] UN General Assembly, Transforming our world: the 2030 agenda for sustainable development, 21 October 2015. https://www.refworld.org/docid/57b6e3e44.html, 2015. (Accessed 28 April 2024).
[2] J. Yang, Y. Ren, S. Chen, Z. Zhang, H. Pang, X. Wang, J. Lu, Thermally activated drinking water treatment sludge as a supplementary cementitious material: properties, pozzolanic activity and hydration characteristics, Constr. Build. Mater. 365 (2023) 130027, https://doi.org/10.1016/j.conbuildmat.2022.130027.
[3] H.B. Dharmappa, A. Hasia, P. Hagare, Water treatment plant residuals management, Water Sci. Technol. 35 (8) (1997) 45–56, https://doi.org/10.1016/S0273-1223(97)00150-9.
[4] UNESCO & UN-Water, United Nations World Water Development Report 2020: Water and Climate Change, UNESCO, Paris, 2020. https://unesdoc.unesco.org/ark:/48223/pf0000372985.locale=en. (Accessed 25 April 2024).
[5] N. Bensitel, K. Haboubi, F.Z. Azar, Y. El Hammoudani, A. El Abdouni, C. Haboubi, A. El Kasmi, Potential reuse of sludge from a potable water treatment plant in Al Hoceima city in northern Morocco, Water Cycle 4 (2023) 154–162, https://doi.org/10.1016/j.watcyc.2023.07.002.
[6] P.N. Pham, W. Duan, Y. Zhuge, Y. Liu, I.E.S. Tormo, Properties of mortar incorporating untreated and treated drinking water treatment sludge, Constr. Build. Mater. 280 (2021) 122558, https://doi.org/10.1016/j.conbuildmat.2021.122558.
[7] S. Sharma, M.M. Ahammed, Application of modified water treatment residuals in water and wastewater treatment: a review, Heliyon 9 (5) (2023) e15796, https://doi.org/10.1016/j.heliyon.2023.e15796.
[8] T. Van Truong, D.J. Kim, Phosphate removal using thermally regenerated Al adsorbent from drinking water treatment sludge, Environ. Res. 196 (2021) 110877, https://doi.org/10.1016/j.envres.2021.110877.
[9] I. Ballou, S. Kounbach, J. Naja, Z.E. Bakher, K. Laraki, F. Raibi, S. Kholtei, A new approach of aluminum extraction from drinking water treatment sludge using ammonium sulfate roasting process, Miner. Eng. 189 (2022) 107859, https://doi.org/10.1016/j.mineng.2022.107859.
[10] J. Ryu, Y.S. Han, D.W. Cho, S.J. Kim, Y.C. Cho, C.M. Chon, I.H. Nam, Practical application of PAC sludge-valorized biochars to the mitigation of methyl arsenic in wetlands, Chem. Eng. J. 450 (2022) 138148, https://doi.org/10.1016/j.cej.2022.138148.
[11] Y. Zhao, A. Nzihou, B. Ren, N. Lyczko, C. Shen, C. Kang, B. Ji, Waterworks sludge: an underrated material for beneficial reuse in water and environmental engineering, Waste Biomass Valorization 12 (2021) 4239–4251, https://doi.org/10.1007/s12649-020-01232-w.
[12] T. Ahmad, K. Ahmad, M. Alam, Sustainable management of water treatment sludge through 3 'R'concept, J. Clean. Prod. 124 (2016) 1–13, https://doi.org/10.1016/j.jclepro.2016.02.073.
[13] A.B. Abba, S. Saggai, Y. Touil, N. Al-Ansari, S. Kouadri, F.Z. Nouasria, K.M. Khedher, Copper and zinc removal from wastewater using alum sludge recovered from water treatment plant, Sustainability 14 (16) (2022) 9806, https://doi.org/10.3390/su14169806.
[14] M.F. Soliman, M.N. Rashed, A.A. Ahmd, Chemical activation of sludge from drinking water treatment plant for adsorption of methylene blue dye, Water Air Soil Pollut. 234 (4) (2023) 228, https://doi.org/10.1007/s11270-023-06216-9.
[15] Y. Yang, Y. Zhao, R. Liu, D. Morgan, Global development of various emerged substrates utilized in constructed wetlands, Bioresour. Technol. 261 (2018) 441–452, https://doi.org/10.1016/j.biortech.2018.03.085.
[16] M.A. Tony, Valorization of undervalued aluminum-based waterworks sludge waste for the science of "The 5 Rs' criteria", Appl. Water Sci. 12 (2) (2022) 20, https://doi.org/10.1007/s13201-021-01554-7.
[17] R. Dias, M.A. Daam, M. Diniz, R. Mauricio, Drinking water treatment residuals, a low-cost and environmentally friendly adsorbent for the removal of hormones-A review, J. Water Process Eng. 56 (2023) 104322, https://doi.org/10.1016/j.jwpe.2023.104322.
[18] D. Nayeri, S.A. Mousavi, A comprehensive review on the coagulant recovery and reuse from drinking water treatment sludge, J. Environ. Manag. 319 (2022) 115649, https://doi.org/10.1016/j.jenvman.2022.115649.
[19] J. Liu, J. Zhang, Z. Dai, B. Li, X. Chen, X. Meng, Recycling aluminum from polyaluminum chloride sludge through acid dissolution and cation resin separation/purification, Water Res. 122096 (2024), https://doi.org/10.1016/j.watres.2024.122096.
[20] N. Nomanifar, M. Davoudi, A. Ghorbanian, A.A. Najafpoor, A. Hosseinzadeh, Fe recovery from drinking water treatment sludge for reuse in tannery wastewater treatment: machine learning and statistical modelling, J. Water Process Eng. 60 (2024) 105224, https://doi.org/10.1016/j.jwpe.2024.105224.
[21] T. Ahmad, K. Ahmad, M. Alam, Simultaneous modelling of coagulant recovery and reuse by response surface methodology, J. Environ. Manag. 285 (2021) 112139, https://doi.org/10.1016/j.jenvman.2021.112139.
[22] A.Y. Bagastyo, A.P. Ayu, R.A. Barakwan, Y. Trihadiningrum, Recovery of alum sludge by using membrane-based electrochemical process, J. Ecol. Eng. 21 (6) (2020) 237–247, https://doi.org/10.12911/22998993/124076.
[23] J. Keeley, P. Jarvis, S.J. Judd, Coagulant recovery from water treatment residuals: a review of applicable technologies, Crit. Rev. Environ. Sci. Technol. 44 (24) (2014) 2675–2719, https://doi.org/10.1080/10643389.2013.829766.
[24] S. De Carvalho Gomes, J.L. Zhou, W. Li, G. Long, Progress in manufacture and properties of construction materials incorporating water treatment sludge: a review, Resour. Conserv. Recycl. 145 (2019) 148–159, https://doi.org/10.1016/j.resconrec.2019.02.032.
[25] F. Azeddine, P.A. Sergio, L. Angélique, L. El Khadir, I. Ali, B. El Houssayne, Rheological behavior and characterization of drinking water treatment sludge from Morocco, Clean Technol 5 (1) (2023) 259–273, https://doi.org/10.3390/cleantechnol5010015.
[26] K. Lebogang, F. Ntuli, T. Lekgoba, V. Kandjou, M. Tsie, Characterization and utilization of water treatment sludge for coagulation of raw water, Water Sci. Technol. 87 (7) (2023) 1587–1599, https://doi.org/10.2166/wst.2023.090.
[27] A.T. Nair, M.M. Ahammed, Influence of sludge characteristics on coagulant recovery from water treatment sludge: a preliminary study, J. Mater. Cycles Waste Manag. 19 (2017) 1228–1234, https://doi.org/10.1007/s10163-016-0513-0.
[28] T. Ahmad, K. Ahmad, M. Alam, Sludge quantification at water treatment plant and its management scenario, Environ. Monit. Assess. 189 (2017) 1–10, https://doi.org/10.1007/s10661-017-6166-1.
[29] M.D. Nguyen, M. Thomas, A. Surapaneni, E.M. Moon, N.A. Milne, Beneficial reuse of water treatment sludge in the context of circular economy, Environ. Technol. Innov. 28 (2022) 102651, https://doi.org/10.1016/j.eti.2022.102651.
[30] ICONTEC, NTC 3903: 2010. Procedimiento para el ensayo de coagulación-floculación en un recipiente con agua o Método de Jarras, in: https://tienda.icontec.org/gp-procedimiento-para-el-ensayo-de-coagulacion-floculacion-en-un-recipiente-con-agua-o-metodo-de-jarras-ntc3903-2010.html, 2010.
[31] L. Di Bernardo, A.D.B. Dantas, Métodos e técnicas de tratamento de agua, second ed., 2005. Sao Carlos, Brasil: RiMa.
[32] Mackenzie L. Davis, Water and Wastewater Engineering: Design Principles and Practice, second ed., McGraw-Hill Education, New York, 2020.
[33] APHA, AWWA, WFE, Standard Methods for Examination of Water and Wastewater, 2017, 23 th. Washington D.C.
[34] ASTM, ASTM D 7573. Standard test method for total carbon and organic carbon in water by high temperature catalytic combustion and infrared detection. https://doi.org/10.1520/D7573-18AE01, 2013.
[35] E.K. Guechi, O. Hamdaoui, Biosorption of methylene blue from aqueous solution by potato (Solanum tuberosum) peel: equilibrium modelling, kinetic, and thermodynamic studies, Desalin. Water Treat. 57 (22) (2016) 10270–10285, https://doi.org/10.1080/19443994.2015.1035338.
[36] S. Kawamura, Integrated Design and Operation of Water Treatment Facilities, second ed., John Wiley and Sons, New York, 2000.
[37] M.R. Vianna, B.O. Ferreira, J.C.M. Filho, Quantification of solids production in potable water treatment plants in Minas Gerais, Brazil: study of two cases, Int. J. Emerg. Tech. Adv. Eng. 4 (9) (2014) 6–12.
[38] American Water Works Association -AWWA- & Edzwald, J, Water Quality & Treatment: A Handbook on Drinking Water, sixth ed., McGraw-Hill Education, New York, 2011.
[39] C.S. Lee, Y.C. Lee, H.M. Chiang, Abrupt state change of river water quality (turbidity): effect of extreme rainfalls and typhoons, Sci. Total Environ. 557 (2016) 91–101, https://doi.org/10.1016/j.scitotenv.2016.02.213.
[40] World Health Organization -WHO-, Water quality and health-review of turbidity: information for regulators and water suppliers, Available online: https://www.who.int/publications/i/item/WHO-FWC-WSH-17.01, 2017. (Accessed 3 May 2024).

[41] B.I. Gandiwa, L.B. Moyo, S. Ncube, T.A. Mamvura, L.L. Mguni, N. Hlabangana, Optimisation of using a blend of plant based natural and synthetic coagulants for water treatment:(Moringa Oleifera-Cactus Opuntia-alum blend), S. Afr. J. Chem. Eng. 34 (2020) 158–164, https://doi.org/10.1016/j.sajce.2020.07.005.
[42] Y. Mao, S. Cotterill, D. Morgan, S. Regan, Y. Zhao, Electrocoagulation of peatland runoff: statistical optimization and economic analysis, J. Water Process Eng. 49 (2022) 103113, https://doi.org/10.1016/j.jwpe.2022.103113.
[43] K.B. Dassanayake, G.Y. Jayasinghe, A. Surapaneni, C. Hetherington, A review on alum sludge reuse with special reference to agricultural applications and future challenges, Waste Manag. 38 (2015) 321–335, https://doi.org/10.1016/j.wasman.2014.11.025.
[44] A. Matilainen, M. Vepsäläinen, M. Sillanpää, Natural organic matter removal by coagulation during drinking water treatment: a review, Adv. Colloid Interface Sci. 159 (2) (2010) 189–197, https://doi.org/10.1016/j.cis.2010.06.007.
[45] R. Gregory, G. Dillon, Minimising sludge production at water-treatment plants, Water Environ. J. 16 (3) (2002) 174–179, https://doi.org/10.1111/j.1747-6593.2002.tb00391.x.
[46] A.C. Ryan, R.C. Santore, S. Tobiason, G. WoldeGabriel, A.R. Groffman, Total recoverable aluminum: not totally relevant for water quality standards, Integr. Environ. Assess. Manag. 15 (6) (2019) 974–987, https://doi.org/10.1002/ieam.4177.
[47] H. Fu, X. Quan, H. Zhao, Photodegradation of γ-HCH by α-Fe_2O_3 and the influence of fulvic acid, J. Photochem. Photobiol., A: Chem 173 (2) (2005) 143–149, https://doi.org/10.1016/j.jphotochem.2005.01.013.
[48] M. Sillanpää, M.C. Ncibi, A. Matilainen, M. Vepsäläinen, Removal of natural organic matter in drinking water treatment by coagulation: a comprehensive review, Chemosphere 190 (2018) 54–71, https://doi.org/10.1016/j.chemosphere.2017.09.113.
[49] T. Turner, R. Wheeler, A. Stone, I. Oliver, Potential alternative reuse pathways for water treatment residuals: remaining barriers and questions—a review, Water, Air, Soil Pollut. 230 (9) (2019) 227, https://doi.org/10.1007/s11270-019-4272-0.
[50] M. Likus, M. Komorowska-Kaufman, A. Pruss, Ł. Zych, T. Bajda, Iron-based water treatment residuals: phase, physicochemical characterization, and textural properties, Materials 14 (14) (2021) 3938, https://doi.org/10.3390/ma14143938.
[51] M. Pająk, Alum sludge as an adsorbent for inorganic and organic pollutants removal from aqueous solutions: a review, Int. J. Environ. Sci. Technol. 20 (10) (2023) 10953–10972, https://doi.org/10.1007/s13762-023-04854-4.
[52] A.F. Gualtieri, S. Ferrari, Kinetics of illite dehydroxylation, Phys. Chem. Miner. 33 (2006) 490–501, https://doi.org/10.1007/s00269-006-0092-z.
[53] G.Z.B. Santos, J.A. Melo Filho, L. Manzato, Proposta de uma cerâmica obtida por meio de geopolimerização de lodo de ETA calcinado, Cerâmica 64 (2018) 276–283, https://doi.org/10.1590/0366-69132018643702353.
[54] W. Smykatz-Kloss, K. Heide, W. Klinke, Chapter 11 - applications of thermal methods in the geosciences, in: Michael E. Brown, Patrick K. Gallagher (Eds.), Handbook of Thermal Analysis and Calorimetry, vol. 2, Elsevier Science B.V, 2003, pp. 451–593, https://doi.org/10.1016/S1573-4374(03)80015-8.
[55] A.T. Nair, M.M. Ahammed, The reuse of water treatment sludge as a coagulant for post-treatment of UASB reactor treating urban wastewater, J. Clean. Prod. 96 (2015) 272–281, https://doi.org/10.1016/j.jclepro.2013.12.037.
[56] A. Suman, T. Ahmad, K. Ahmad, Dairy wastewater treatment using water treatment sludge as coagulant: a novel treatment approach, Environ. Dev. Sustain. 20 (2018) 1615–1625, https://doi.org/10.1007/s10668-017-9956-2.
[57] M. Ayoub, H. Afify, A. Abdelfattah, Chemically enhanced primary treatment of sewage using the recovered alum from water treatment sludge in a model of hydraulic clari-flocculator, J. Water Process Eng. 19 (2017) 133–138, https://doi.org/10.1016/j.jwpe.2017.07.014.
[58] T. Chakraborty, M. Gabriel, A.S. Amiri, D. Santoro, J. Walton, S. Smith, G. Nakhla, Carbon and phosphorus removal from primary municipal wastewater using recovered aluminum, Environ. Sci. Technol. 51 (21) (2017) 12302–12309, https://doi.org/10.1021/acs.est.7b03405.
[59] T. Chakraborty, D. Balusani, S. Smith, D. Santoro, J. Walton, G. Nakhla, M.B. Ray, Reusability of recovered iron coagulant from primary municipal sludge and its impact on chemically enhanced primary treatment, Sep. Purif. Technol. 231 (2020) 115894, https://doi.org/10.1016/j.seppur.2019.115894.
[60] ASTM, ASTM D2487-11. Standard practice for classification of soils for engineering purposes. https://doi.org/10.1520/D2487-11, 2011. ASTM D2487-11.
[61] J. Lyklema, Nomenclature, symbols, definitions and measurements for electrified interfaces in aqueous dispersions of solids (Recommendations 1991), Pure Appl. Chem. 63 (6) (1991) 895–906, https://doi.org/10.1351/pac199163060895.
[62] D.S. Martins, B.R. Estevam, I.D. Perez, J.H.P. Américo-Pinheiro, W.D. Isique, R.F. Boina, Sludge from a water treatment plant as an adsorbent of endocrine disruptors, J. Environ. Chem. Eng. 10 (4) (2022) 108090, https://doi.org/10.1016/j.jece.2022.108090.
[63] E.K. Jeon, S. Ryu, S.W. Park, L. Wang, D.C. Tsang, K. Baek, Enhanced adsorption of arsenic onto alum sludge modified by calcination, J. Clean. Prod. 176 (2018) 54–62, https://doi.org/10.1016/j.jclepro.2017.12.153.
[64] M. Shamaki, S. Adu-Amankwah, L. Black, Reuse of UK alum water treatment sludge in cement-based materials, Constr. Build. Mater. 275 (2021) 122047, https://doi.org/10.1016/j.conbuildmat.2020.122047.
[65] M. Everaert, J. Bergmans, K. Broos, B. Hermans, B. Michielsen, Granulation and calcination of alum sludge for the development of a phosphorus adsorbent: from lab scale to pilot scale, J. Environ. Manag. 279 (2021) 111525, https://doi.org/10.1016/j.jenvman.2020.111525.
[66] S.R. Teixeira, G.T.A. Santos, A.E. Souza, P. Alessio, S.A. Souza, N.R. Souza, The effect of incorporation of a Brazilian water treatment plant sludge on the properties of ceramic materials, Appl. Clay Sci. 53 (4) (2011) 561–565, https://doi.org/10.1016/j.clay.2011.05.004.